Accepted Manuscript

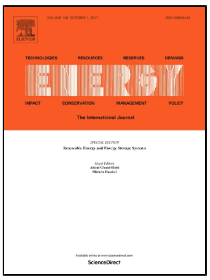

Assessment of the intra-annual and inter-annual variability of the wave energy resource in the Bay of Biscay (France)

Joan Pau Sierra, Adam White, Cesar Mösso, Marc Mestres

PII:	S0360-5442(17)31632-8
DOI:	10.1016/j.energy.2017.09.112
Reference:	EGY 11606
To appear in:	*Energy*
Received Date:	12 June 2017
Revised Date:	22 September 2017
Accepted Date:	24 September 2017

Please cite this article as: Joan Pau Sierra, Adam White, Cesar Mösso, Marc Mestres, Assessment of the intra-annual and inter-annual variability of the wave energy resource in the Bay of Biscay (France), *Energy* (2017), doi: 10.1016/j.energy.2017.09.112

- Wave power in the French Atlantic coast is assessed using a 58-year series of data
- Considerable wave energy power is detected similar to nearby areas
- Large inter-annual and intra-annual variability of wave power is found
- The power output for 2 WECs (Wave Dragon and Pelamis) is computed
- Points with greater wave power are not necessarily those with greater WEC output

Assessment of the intra-annual and inter-annual variability of the wave energy resource in the Bay of Biscay (France)

Joan Pau Sierra[1,2,*], Adam White[1,3], Cesar Mösso[1,2] & Marc Mestres[1,2]

[1]*Laboratori d'Enginyeria Marítima,Universitat Politècnica de Catalunya BarcelonaTech , Jordi Girona 1-3, Mòdul D1, Campus Nord, 08034 Barcelona, Spain*

[2]*Centre Internacional d'Investigació dels Recursos Costaners, Jordi Girona 1-3, Mòdul D1, Campus Nord, 08034 Barcelona, Spain*

[3]*Now at AECOM, 1 Tanfield, EH3 5DA Edinburgh, UK*

[*]Corresponding author: *joan.pau.sierra@upc.edu; tel. +34 934016467; fax: +34 934011861*

adamzwhite93@gmail.com

cesar.mosso@upc.edu

mmestresridge@gmail.com

Abstract

In this paper, the wave energy potential in the western coast of France is assessed, analyzing 58 years of data from numerical models at 10 points located between latitudes 43º30'N and 47ºN. The study focuses on the temporal variability at different scales (monthly, seasonal and inter-annual). The northern part of this stretch is the most energetic (wave powers greater than 22 kW/m), with a decrease of the wave power southwards. The results show that both the wave power resource and the energy output of two wave energy converters (WECs) at the Atlantic coast of France have strong intra-annual and inter-annual variability. From one year to another the wave power may present variations of up to 200%, and the WEC energy output may almost double. These results illustrate that the average mean power alone is not sufficient for adequate wave resource quantification, and it is necessary to consider the intra-annual and inter-annual variability of the wave power and the WEC output when analyzing the potential installation of a wave energy farm in a certain area.

1. Introduction

The European Union (EU) countries, which have limited fossil fuel deposits, consume one fifth of the world's oil and gas supplies, spending billions of euros every year to buy those commodities from third countries [1]. In 2009 the EU adopted the directive 2009/28/EC, which stipulates that by 2020, 20% of EU final energy consumption must be obtained from renewable sources and the greenhouse gas emission should be reduced by 30% [2]. To achieve this goal, in the last years renewable energies have been boosted in European countries, increasing their share of gross energy consumption from 5% in 1999 to 14.9% in 2013 [3].

Marine renewable energy sources are among the most auspicious due to their higher power density [4] and the existence of large water areas, which can be used to develop extensive marine energy parks [5]. In particular, wave energy may be harvested in many more potential sites than tidal energy, which needs strong currents generally restricted to a small number of coastal areas like estuaries or shallow-water straits [6-7].

The Northeastern Atlantic area presents one of the largest wave energy resources in the world [8] exceeding 40 kW/m in many areas [9]. In this region, wave power has been studied around islands like the Canary Islands [10-12], Madeira [13-14], Azores Islands [15] or British Isles [16-17], and in the continental coasts of Africa [18] or Europe, mainly in Portugal (e.g. [19-21]), Spain (e.g. [6,22-24]) and France [7,25-26], or larger areas covering several countries [5,27]. These analyses have confirmed the high wave energy potential of the north-western European shelf area. Despite wave energy being subject to strong seasonal and inter-annual variations [27], most of these studies have focused only on the mean energy potential, devoting less attention to its temporal variability. However, these fluctuations of the energy resource can appreciably reduce the efficiency of a device designed to work under average conditions [28-29].

Therefore, resource variability can play an important role in the cost-efficiency balance [30], and it is also a decisive factor for selecting adequate locations from a technical standpoint [31]. An ideal wave energy plant would supply relatively constant power throughout time, but this is precluded by the resource's temporal variations [32]. The considerable uncertainty associated to inter-annual and inter-seasonal variability of the wave power resource is one of the factors that is slowing down the progression of full scale prototypes and pre-commercial devices towards commercial arrays of wave energy converters (WECs) [4,33].

As pointed out in several studies [29,34-35], one of the main disadvantages of wave energy, given the random nature of waves, is its large variability at different time scales (wave to wave, sea state, monthly, seasonal and inter-annual variations) [30]. In addition, a recent study has stated that, due to temporal variations, the areas with high amounts of wave energy are not necessarily the optimal locations for wave energy harvesting [28].

Different researchers have studied wave climate variability at several temporal scales (e.g. [30,36-39]), although most of them are based on periods of a few years, which are too short to capture the inter-annual variability during the entire life cycle of a WEC. Nevertheless, some studies have pointed out decadal changes in wave height based on satellite observations and numerical data (e.g. [28,30,32,38]).

This study presents an assessment of the wave power resource using a long time series of wave data (58 years) and focusing on the variability of such resource at different time scales (monthly, seasonal and inter-annual). In addition, it analyzes the inter-annual variation of the wave energy output provided by two WECs. The research is focused on a stretch of the Atlantic French coast, the Bay of Biscay, in the area between Brittany and the Spanish border. Several previous studies have assessed the wave resource potential in nearby areas: the southern area of this Bay in the Spanish coast [20,24] and its northern part in the Sea of Iroise around Brittany [7,26]. Other studies [25,27] have assessed the wave power resource in the same area, but they use shorter time series of wave data (3 and 7 years respectively).

The paper is structured as follows: In Section 2, the used data and methodology are detailed, while in Section 3 the wave data are analyzed. In Section 4 the average (in the 58-year period) results of wave power and WEC performance in the study area are presented. In Section 5 the same results are analyzed taking into account the temporal variability at different scales. Lastly, in Section 6 the main conclusions of this work are summarized.

2. Data and methods

2.1. Study area and available wave data

The Bay of Biscay is a gulf of the northeast Atlantic Ocean stretching along the western coast of France and the northern coast of Spain. In this study, only the French coast of this

bay located south of Brittany is analyzed. The study area includes the Atlantic coast of France between latitudes 43º30'N and 47°N.

The data used for this study were provided by the Spanish Harbour Authority (*Puertos del Estado*) and correspond to the 58-year SIMAR database. This database consists of two subsets: the first one (1958-1999) includes hindcasting wave data obtained during the European HIPOCAS project [40-41] using the WAM numerical model [42], which was fed by the winds given by the REMO regional circulation model (RCM) [43]. This RCM was forced by the global reanalysis performed by the U.S. National Centers for Environmental Prediction (NCEP). The spatial resolution of the HIPOCAS database is 0.25º X 0.25º, while the time interval between data is 3 h. The different parameters involved in the simulation process have been widely validated [41,44-45]. This simulation has some limitations in terms of properly reproducing certain storm events, but it generally replicates mean values quite well [46]. This database was validated by [41] using measured data from wave buoys at different points of the Atlantic European coast. For the Bay of Biscay they found values of the bias between -0.003 and -0.631 for the significant wave height (H_s) and between -0.136 and 0.320 for the mean wave period (T_m). The scatter index for H_s ranged between 0.261 and 0.460 and between 0.160 and 0.185 for T_m. The Pearson's correlation coefficient varied between 0.899 and 0.960 for H_s and between 0.774 and 0.826 for T_m. In addition, data from the HIPOCAS database have been used to assess the wave energy resource in different areas (e.g. [6,11,23-24]).

The second subset of data (2000-2015) is a forecasting wave climate database generated also using the WAM model [42], but in this case the RCM used is the HIRLAM model [47], which is run by the Spanish Meteorological Agency. For each time step, the model provides wind and pressure fields consistent with the previous evolution of modeling parameters and with physical observations. This data subset has also been used in previous studies of the wave energy resource [48]. In this line, hindcasted wave data have been widely used to assess wave energy potential (e.g. [8,28,49]).

The analysis of the wave energy is focused on 10 points distributed between the aforementioned latitudes and whose location is shown in Figure 1. All the points have been selected trying to minimize the distance to the coast (which ranges between 8 and 47 km) and having a minimum water depth which allows the WEC deployment (all of them are located at depths greater than 50 m with two exceptions: P4 at 38 m and P9 at 40 m. Other points located farther from the coast could have been selected for the analysis, because their energy potential should be greater due to less wave dispersion (both in direction and frequency) and bottom friction. Nevertheless, the larger the distance to the coast, the greater the costs of the connection to the grid, since more cable is necessary and, in addition, the points located farther offshore have larger water depths, increasing the mooring costs too. Therefore, for these farther points, it is necessary to make a balance between the costs and the energy harvested and this was not the goal of this work. For this reason, the analysis is limited to the points closest to the coast having a minimum water depth.

2.2. Methodology

The wave power (P) per unit width (units of kW/m) in deep-water is computed as a function of the seawater density (ρ, for which a value of 1025 kg/m^3 is considered), the gravity (g), H_s and the energy period (T_e):

$$P = \frac{\rho g^2}{64\pi} H_s^2 T_e \approx 0.491 H_s^2 T_e \quad (1)$$

The value of T_e depends on the spectral moments:

$$T_e = \frac{m_{-1}}{m_0} \quad (2)$$

where m_0 and m_{-1} are the 0-th order and -1th order spectral moments.

The SIMAR database does not provide information on spectral moments or T_e. For this reason, T_e is assessed from the peak period (T_p) following [49], as:

$$T_e = \alpha T_p \quad (3)$$

where α is a coefficient whose value depends on the wave spectrum shape, varying between 0.86 (for wide-band spectra) and 1 (for narrow-band spectra). In the studied area, both types of sea states (sea and swell) are relevant, so a wide range of coefficient α values can be expected. In this work, following the suggestion of [49], a value α = 0.9 (which can be considered conservative) was adopted to compute the wave power.

For some sea states (those with longer periods) the deep-water assumption is not fulfilled and, therefore, the use of equation (1) introduces certain inaccuracy. Despite this, considering the uncertainty contained in equation (3) and the conservative value of α assumed to compute T_e, the error committed when using (1) in these cases can be deemed admissible. Therefore, the mean wave power at each point can be computed using equations (1) and (3) for each one of the 58 years and for the total time span.

Besides the available average wave power, another aspect to take into account when considering a site for WEC installation is the temporal variation of energy at different scales (daily, monthly, seasonal and annual). Locations with smaller oscillations of the energy flux are better for this purpose than those with highly variable wave conditions, because the energy supply is more constant and the device efficiency improves. In addition, as pointed out in [28], the feasibility of wave energy harvesting projects resides in the optimum design of WECs, which should take into account the variability of the resources and not be based solely on their mean value.

In this work, the temporal variability of wave power at each point is estimated using the three coefficients proposed by Cornett [49]: the coefficient of variation (COV), the seasonal variability index (SV) and the monthly variability index (MV). The first one analyzes the temporal variability of the wave power time series by obtaining the ratio between its standard deviation and its average value. SV computes the variability on a seasonal basis as the ratio between the difference of the average wave power for the highest-energy and the lowest-energy seasons over the annual mean wave power. Finally, MV estimates the variability on a monthly basis by making computations similar to those of SV but using the average wave power of the highest-energy and the lowest-energy months. For each coefficient, the greater its value the larger the temporal variability associated to its time scale.

In addition, and considering the long-term data set available, an equivalent index is introduced to assess annual variations. The annual variability index, AV, is defined thus as:

$$AV = \frac{P_{Y,\max} - P_{Y,\min}}{P_{year}} \quad (4)$$

where P_{year} is the yearly mean wave power, $P_{Y,max}$ is the mean wave power for the highest-energy year and $P_{Y,min}$ is the mean wave power for the lowest-energy year of the analyzed

period, in this case 58 years. The greater the value of AV, the larger the annual variability, being AV = 0 the ideal value, since it would mean that each year has the same amount of wave power.

Besides the temporal variability, another essential consideration for the installation of a wave energy farm is the quantity of wave energy yielded by a WEC. This depends not only on the available wave energy, but also on how this energy is distributed between energy bins, which are defined by intervals of T_e and H_s [13]. The reason for this is that each WEC has a different power matrix, which indicates the amount of energy harvested for each bin. Therefore, each WEC has its best performance for a certain range of wave heights and wave periods and, at a given location, some WECs will be more suitable than others, depending on the characteristics of the waves. The energy output of a WEC for a particular energy bin is obtained by multiplying the number of hours per year corresponding to this bin by the electric power provided in the WEC's power matrix for the same bin. The total annual energy yielded by the WEC is obtained by adding the energy output of all the bins.

Herein, the energy harvested is assessed for two WECs in an advanced development stage: Pelamis [50], whose principle is attenuator, and Wave Dragon [51], whose principle is terminator. Their efficiency can be estimated through the capacity factor, which is an index giving the ratio between the average electric power yielded by the WEC and its maximum rated power. Both magnitudes (wave energy output and capacity factor) are computed for each year and also as the average of the whole studied period.

3. Analysis of wave data

Previously to the wave power assessment, the main wave features in the study area are analyzed. In Figure 2, the mean H_s and T_e for the 58-year period at the 10 studied points are plotted. The results shown in this figure indicate that the largest H_s are located in the northern stretch of the studied area and the lowest at the south, while the central section presents intermediate values. On the contrary, the mean energy period tends to increase southwards.

The H_s mean values are around 1.80 m in the northern sector (points P1 to P3), slightly lower than 1.70 m in the central stretch (points P4 to P7) and between 1.62 m and 1.52 m in the south (points P8 to P10). As regards T_e, the lowest mean value is found at P1 with 8.6 s, gradually increasing to the south, with a maximum value of 9.2 s at P10. This suggests that swell waves increase their presence towards the southern sector.

The inter-annual variability of H_s and T_e is illustrated in Figure 3, in which the average value of both parameters at each year of the 58-year period is shown for two points, P1 and P5. Significant changes of the mean H_s are observed, since its values range between 1.37 m and 2.13 m at P1 and between 1.39 m and 1.97 m at P5. Therefore, the values of the average H_s may vary up to 42% (P5) or 55% (P1) from one year to another. On the contrary, the inter-annual changes in mean annual T_e values are of less magnitude, oscillating between 7.9 s and 9.7 s at P1 (differences of up to 23%) and between 7.7 s and 10 s at P5 (differences up to 30%). Taking into account these values and that the wave power P is a function of the square of H_s, it is obvious that the inter-annual variations of P are mainly due to this wave height variability.

The intra-annual variability of H_s and T_e is also analyzed at two different scales: monthly (Figure 4) and seasonal (Figure 5). The H_s follow a similar pattern in all points, with maximum values in the winter months (January, December and February in this order), followed by November and March. On the contrary, from May to September, the values of H_s are considerably smaller. The ratio between the largest monthly-averaged H_s (January) and the smallest (July) ranges between 2.42 (at P1) and 2.12 (at P9). At a seasonal scale, the

greatest H_s take place in winter (with values between 2.54 m at P2 and 2.06 m at P9), while in summer the values are the lowest (between 1.15 m at P2 and 1.02 m at P9), as it could be expected. The ratios of maximum vs minimum seasonally-averaged H_s range between 2.23 at P1 and 2.02 at P9). In spring and autumn, the average values of H_s are very similar at all the points, being intermediate between those of summer and winter, with values between 1.5 m and 1.8 m. A general trend of decreasing mean values of H_s from North to South is observed, indicating that the northern points receive more energetic waves.

With regard to T_e, the monthly patterns are similar to those of H_s, with greatest average values in winter (between 9.7 s and 10.7 s) than in summer (between 7.2 and 7.9 s) and intermediate values in spring and autumn. The main difference with respect to H_s is that, in this case, an increasing trend of all the seasonally-averaged values of T_e is observed southwards in consistence with the mean annual values (Figure 2). This seems to confirm the increasing presence of swells towards the southern sector of the studied area.

The wave roses at four points (distributed along the studied stretch) are plotted in Figure 6, showing the directional distribution of H_s. Almost all the waves in this area come from the sector between the W and NW, although a progressive turning of the wave direction from W to NW is observed when going to the south. Thus, at P1 39% of the waves are from the W and 27% from the WNW, while at P5 25% are from the W, 48% from the WNW and 14% from the NW. At P8, 57% of the waves come from the WNW and 27% from the NW and at P10, 44% are from the WNW and 47% from the NW.

4. Assessment of the average wave power and energy output

In this section the results are obtained considering the complete data set (58-year series) and computing average values representative of the entire period. These mean values will be compared with those accounting for the inter-annual variability, which will be presented in the next section

The average wave power for the entire period at all the studied points is presented in Figure 7 and Table 1. The wave power is comparable at all points, although the three northernmost locations have slightly larger values, with the mean wave power ranging between 22.6 and 23.8 kW/m. The other points (with the exception of P9 with 17.5 kW/m) have similar wave power values, varying between 19.7 and 20.8 kW/m. These values are consistent with those found in the SE Bay of Biscay (northern Spanish coast) in [24], where an average wave power of about 25 kW/m was computed. They are also coincident to those obtained by [7] in Brittany (at the north of this study area), who found values between 15 kW/h in coastal areas and 40 kW/m offshore, and [25] in this area, where the wave power ranged between 20-25 kW/m.

Besides the average energy available, a crucial aspect for evaluating the suitability of a particular site for WEC deployment is the energy that can be harvested by an installed device. As indicated in Section 2.2, this energy output depends on how the resource is distributed among energy bins. For this reason, the scatter diagrams of H_s and T_e have been determined for the 10 locations to compute the energy output. In Figure 8, some of these scatter diagrams are shown.

In Figure 8, the total annual energy (in MW h/m) that could potentially be harvested from each sea state (at intervals of 0.5 m for H_s and 1 s for T_e) is shown. These plots allow identifying the bins with the greatest energy potential. At all points the largest-energy source is concentrated in the band of T_e ranging between 10 and 12 s and H_s between 2 and 4 m.

Using the scatter diagrams and the WEC power matrices (which were obtained from Ref [14]), the energy output of both WECs can be computed. These values are summarized in Table 1 and plotted in Figure 9.

From the analysis of Figure 9 and Table 1, differences between both WEC outputs can be observed. The energy delivered by the Wave Dragon ranges between 15.7 and 17 GW h per year, while for the Pelamis the energy harvested is about 1 GW h per year. The highest annual energy output for both the Pelamis and the Wave Dragon WECs correspond to the three northernmost points (those with the largest wave power), although locations P5 and P6 yield also similar energy output for the Wave Dragon. The Pelamis converter shows a clear decreasing productivity from north to south (with the exception of point P4), while this trend does not exist for the Wave Dragon, for which the central stretch of the studied area yields energy levels similar to those of the northern sector.

To conclude the analysis of the average values, the average capacity factor (during the entire period) for both WECs is assessed as a measure of their efficiency. The values of these capacity factors are presented in Figure 10 and Table 1. In the northern and central parts of the studied coast, the Wave Dragon attains capacity factors greater than 26.7% (except at P4 where it only reaches 25.4%) decreasing towards the south, with values between 23.9% and 25.9%. The capacity factors for the Pelamis are lower ranging between 11.9% and 16.3%, showing the same decreasing trend from north to south.

5. Assessment of the intra-annual and inter-annual variability

Besides the spatial distribution of the wave energy shown in Figure 7, it is also interesting to examine the temporal variability of the wave power. Since a long time series of data is available (58 years), in this section the wave power variations along the full series are also analyzed at different time scales (monthly, seasonal, yearly).

5.1. Intra-annual variability

In Figure 11, the monthly wave power (averaged over the 58-year period) at the 10 analyzed points is shown. The largest values of energy power are observed in the winter months (December-February), being maximum in January (values between 35.4 kW/m at P9 and 50.4 kW/m at P2). In the summer months (June-August) the wave power has its minimum values, being July the less energetic month (values between 5.1 kW/m at P9 and 6.4 kW/m at P2). March, October and November are also fairly energetic, with powers between 19 kW/m and 31 kW/m), while May and September are rather mild (between 9 kW/m and 12 kW/m) and April is a month of transition (wave powers between 15 kW/m and 18.6 kW/m).

The seasonal wave power (averaged in the 58-year period) at the 10 study points is shown in Figure 12, confirming the marked seasonal character of the wave energy in the study area. Thus, on average, 48% of the annual wave power is concentrated in winter, 23% in autumn (September-November), 22% in spring (March-May) and 7% in summer. These results stress the large seasonal variability since the wave energy potential is almost seven times larger in winter than in summer.

Therefore, four periods with different wave power features can be differentiated during the year: an energetic period from November to March, with monthly averages greater than 24 kW/m at all the points and about 70% of the annual wave energy; a mild interval from May to September with monthly averages lower than 12 kW/m at all the points and 15% of the total wave power; and two periods of intermediate wave energy conditions (October and April)

with monthly averages between 15 kW/m and 23 kW/m depending on the point and representing about 15% of the annual wave power.

To complete this Section, the variability coefficients mentioned in Section 2.2 have been calculated and their values are presented in Table 2 and Figure 13. The four coefficients COV, SV, MV and AV show a decreasing tendency from the north to the center of the study area and an increase from this to the south, with some exceptions. In particular, the temporal variability at point P4 is larger for all the time scales than the variability at its neighbouring northern point P3. In the same way, P9 presents a temporal variability slightly lower than P8 at monthly and seasonal scales and greater than P10 at annual time scale. In general, the temporal variability is large, with values of COV ranging between 1.76 and 1.84, MV from 1.72 to 1.86 and SV from 1.57 to 1.70. AV varies between 0.91 and 1.09, except at P5, where a surprisingly low value (0.77) is obtained.

5.2. Inter-annual variability

The yearly fluctuations are illustrated in Figure 14, which shows the average annual wave power for each year of the series at two points, those presenting the highest and lowest inter-annual variability (P1 and P5, respectively). This figure is complemented by Table 3, in which the mean annual energy values for the full 58-year period, the most energetic year (P_{Y1}), the less energetic year (P_{Y58}) and the ratio of the two latter values (P_{Y1}/P_{Y58}) are shown for each studied point. Figure 14 and Table 3 evidence the large inter-annual variability existing in this area, because the wave power potential at a given point in two different years may vary by a factor of up to three. It is interesting to notice that the inter-annual variation is minimal in the central sector (points P5 and P6, with ratios P_{Y1}/P_{Y58} lower than 2.5). This variability increases towards the north and the south, peaking at both edges (values of P_{Y1}/P_{Y58} around 2.7 or larger), being maximum at P1 (3.08).

To analyze this large inter-annual variability of wave power, box-whisker plots are used. The box-whisker plot describes a set of numerical data through their quartiles in a simple way. It consists of a box, whose edges are the upper (third) and lower (first) quartiles of the dataset. Inside the box there is a band indicating the median (or second quartile). Outside the box, there are two vertical lines (named whiskers) extending up to the minimum and maximum values found in the dataset.

One of these plots is presented in Figure 15, which shows the inter-annual variability. The range of variation between the maximum and minimum annual wave power is similar at all points, except at P1 and P2 where it is significantly larger and at P5, where it is smaller. At all points (except at P5), the years with wave power larger than the upper quartile are those with a greater range of variation. This indicates that the most energetic years are those showing a more irregular distribution of the wave power. On the contrary, those located between the second and the third quartiles and, in particular, those between the first and the second quartile are the years having a more similar wave power.

In addition to the year-to-year variation of the wave power, the month-to-month variation is also analyzed. In Figure 16, the results of the wave power for each month of every year are presented, for points P1 and P5. These results show that the months between April and September have a more regular behavior. On the contrary, the most energetic periods (January-March and October-December) present strong variations of the average monthly wave power, at both intra-annual and inter-annual scales.

This strong intra-annual and inter-annual monthly variability is illustrated in Table 4 in which, for each point, the values of the maximum and minimum monthly wave power for the period of 58 years (696 months) are presented. The range of variation between extremes is very

large, varying for each point from minimum values lower than 2 kW/m to maximum values greater than 100 kW/m. In the northernmost points (P1 to P4) the ratio between the wave power of the most and the less energetic months is greater than 95, while in the other points ranges between 55 (P8) and 67 (P5).

The intra-annual monthly fluctuations are also analyzed and summarized in the last column of Table 4, where the ratios between the most and the less energetic months in the same year are presented. This intra-annual variability is also very large, in particular for the stretch including points P1 to P4, where the average ratios range between 18.7 and 21.3, and the maximum ratios between 59.3 and 74. In the other points, the average ratio ranges between 16.2 and 17.7, and the maximum ratios between 37.5 and 44.7. Both the inter-annual and intra-annual monthly variability present a general decreasing trend from north to south, from P1 to P8, where this trend reverses.

The seasonal inter-annual changes are shown in Figure 17, where the box-whisker plots for the seasonal wave power at each point are drawn. The largest variability is observed in winter followed by autumn, while in spring and, in particular, in summer the variability is significantly lower. As in the case of the yearly analysis, the greatest deviations are observed above the upper quartile, indicating again that the most energetic periods (i.e. with stronger storms) are those with the largest irregularity.

The information contained in Figure 17 is completed with Table 5, in which the seasonal variability of wave power is summarized, including the minimum and maximum values for each season in the 58-year period. For the studied interval, the maximum variability in winter, spring and summer wave power values is observed in the northern stretch of the study area (points P1 to P3), while the autumn variability is larger in the central area (points P5 to P7). On the other hand, as in the case of the monthly analysis, the most energetic seasons (winter and autumn) are also those having larger fluctuations in the wave power values, while the mildest one (summer) presents a more uniform behavior.

In addition, in Table 5 the ratios between the most and the less energetic seasons in the same year (i.e. winter and summer, respectively) are included. These ratios are greater at the northernmost stretch (points P1 to P4) and the southernmost point (P10), with average ratios exceeding 7, and maximum ratios greater than 16.5. At the other points (P5 to P9), the average ratios vary between 6.4 and 6.7, and the maximum ratios between 14.9 and 16.2.

The analysis of the inter-annual changes has been extended to the energy harvested every year by the two WECs considered in this study. In Figure 18, the box-whisker plots obtained at each point from the yearly values of the energy output from the two WECs are shown, while in Table 6 the maximum and minimum annual values and the ratio between them are included. These results present features that differentiate them from those corresponding to the wave power, in which the ratio between the most and the less energetic years varies between 2.2 and 3.1 depending on the site (Table 3). In the case of the energy delivered by the WECs, this ratio is considerably lower and ranges between 1.7 and 1.9 for the Pelamis and between 1.67 and 1.8 for the Wave Dragon.

Another noticeable difference observed with respect to the wave power is that the largest variability in the energy output is found below the lower quartile instead of above the upper one. This means that, unlike in the case of wave power, the years with less energy harvest present the greatest variability in energy output.

The reduction in the ratio between the most and the less energetic years and the largest variability in the milder years for the WECs energy output with respect to the wave power indicates that WECs act as a filter. Indeed, the most energetic sea states are included in the assessment of the wave power, but do not contribute to the energy production since they fall

out of the WEC operation range, and are only important to evaluate the survivability of the converter. This should be taken into account when assessing the wave power in a certain area.

6. Summary and conclusions

In this study, the wave energy resource along the Atlantic coast of France between Brittany and Spain is estimated using a 58-year series of data from numerical modeling (hindcasting and forecasting).

The wave energy potential is assessed using data from 10 points located between latitudes 43º30'N and 47ºN. The average wave power in the area is appreciable (up to 23.8 kW/m), while the average annual wave energy attains values up to 208.8 MW h/m, which is of the same order of magnitude as that found by other studies in nearby areas.

The spatial sharing of wave power along France's Atlantic coast shows little variability, with a higher-energy sector in the northern part of this area (between latitudes 46ºN and 47ºN) and a decreasing trend southwards. Most of the energy is concentrated in sea states with T_e between 10 and 12 s and H_s between 2 and 4 m. With respect to wave direction, the most energetic waves are from W, WNW and NW and a progressive turning of the wave direction from W to NW is observed when moving southwards.

The temporal variability of wave power (averaged over the 58-year period) along the study area shows a marked seasonal sequence, with an energetic winter (48% of the energy, on average), a calm summer (7%) and moderate-energy spring and autumn (with 22% and 23% respectively). There is also an appreciable variability on a monthly basis, with January, December and February being the most energetic months and July, August and June the mildest ones.

The most relevant findings of this work are related to the importance of considering the temporal variability at different scales (monthly, seasonal and yearly) when assessing the wave resource. Thus, there can be a factor of up to three between the annual wave power evaluated at a same point for two different years. The intra-annual fluctuations are also remarkable, since the ratio between the wave power of the most and the less energetic months in the same year varies between 6 (minimum at P9) and 74 (maximum at P1), while the ratio between the wave power of the most and the less energetic seasons in the same year varies between 2.2 (minimum at P9) and 18 (maximum at P1).

If the inter-annual changes during the 58-year period are considered, the fluctuations in the wave power increase. Indeed, the ratio between the wave power of the most and the less energetic months at each point during the entire period ranges between 55 (P8) and 159 (P1), while the ratio between the wave power of the most and the less energetic seasons at each point during the entire period varies between 24.5 (P5) and 36.3 (P1). Therefore, as pointed out by other authors [28,31] the average value of wave power over the entire dataset (58 years in this case) is only a rough indicator of the wave energy potential at a certain place. These results illustrate the need of considering the intra-annual and inter-annual variability of the wave power when assessing it for the potential deployment of WECs, because its magnitude may vary significantly not only from one month to another but also on a yearly basis.

Finally, taking into account the power matrices of two WECs (Pelamis and Wave Dragon), the energy output is computed at the 10 studied points. The average annual energy production for the entire period is obtained, ranging between 0.79 GW h (P9) and 1.07 GW h (P2) for the Pelamis and 14.67 GW h (P10) and 17.02 GW h (P2) for the Wave Dragon.

Performing the analysis on a year by year basis, it is found that the inter-annual variability of the annual wave energy output generated by the two studied WECs is considerably lower (<1.9) than the fluctuations of the annual wave power (between 2.2 and 3). Another interesting result is that the largest variations in the annual energy output are concentrated below the lower quartile (i.e. in the less energetic years) instead of above the upper one (i.e. the most energetic years) as in the case of the annual wave power. This indicates that the most energetic sea states that are considered in the assessment of the wave power do not contribute to the energy generation because they fall out of the WEC operation range. This is a crucial point because the points with a greater wave power potential are not necessarily the best for WEC deployment in terms of energy output. Thus, for example, P1 yields the second greatest wave power value, but only the fourth largest amount of energy harvested by the Wave Dragon converter. Consequently, for the development of a wave energy project in a certain area, not only the wave power and its spatial and temporal variability have to be assessed but also the specific performance of a particular WEC at this place, including the energy output and its temporal variability.

Acknowledgements

This study was funded by the research project “Desarrollo de una herramienta de alta resolución como soporte al diseño, colocación y explotación de instalaciones para energías marinas (DARDO)” (ref. ENE2012-38772-C02-02) funded by the Spanish Ministry of Economy and Competitiveness. The authors are also grateful to the Spanish Port Authority (Organismo Público Puertos del Estado) for providing the wave data. The support of the Secretaria d'Universitats i Recerca del Dpt. d'Economia i Coneixement de la Generalitat de Catalunya (Ref 2014SGR1253) is also acknowledged.

References

[1] EU. Energy: sustainable, secure and affordable energy for Europeans. The European Union Explained. European Commission, Directorate-General for Communication Publications; Brussels; 2012.

[2] European Renewable Energy Council (EREC). Renewable Energy in Europe-Markets, Trends and Technologies; 2010.

[3] European Environmental Agency (EEA), Renewable energy in Europe - approximated recent growth and knock-on effects. EEA Technical Report no 1/2015; 2015.

[4] Clément A, McCullen P, Falcão A, Fiorentino A, Gardner F, Hammarlund K, et al. Wane energy in Europe: current status and perspectives. Renew Sustain Energy Rev 2002;6:405-31.

[5] Rusu L, Onea F. Assessment of the performances of various wave energy converters along the European continental coasts. Energy 2015;82:889-904.

[6] Iglesias G, Carballo R. Wave energy potential along the Death Coast (Spain). Energy 2009;34:1963-75.

[7] Guillou N, Chapalain G. Numerical modelling of nearshore wave energy resource in the Sea of Iroise. Renew Energy 2015;83:942-53.

563 [8] Gunn K, Stock-Williams C. Quantifying the global wave power resource. Renew Energy
564 2012;44:296-304.

565 [9] Pontes MT. Assessing the European wave energy resource. J Offshore Mech Art Eng
566 1998;120:226-31.
567
568 [10] Iglesias G, Carballo R. Wave power for La Isla Bonita. Energy 2010;35:513-21.

569 [11] Sierra JP, González-Marco D, Sospedra J, Gironella X, Mösso C, Sánchez-Arcilla A.
570 Wave energy resource assessment in Lanzarote (Spain). Renew Energy 2013;55: 480-9.

571 [12] Iglesias G, Carballo R. Wave resource in El Hierro an island towards energy self-
572 sufficiency. Renew Energy 2011;36:689-98.
573
574 [13] Rusu E, Pilar P, Guedes Soares C. Evaluation of the wave conditions in Madeira
575 Archipelago with spectral models. Ocean Eng 2008;35:1357-71.

576 [14] Rusu E, Guedes Soares C. Wave energy pattern around the Madeira Islands. Energy
577 2012;45:771-85.

578 [15] Rusu L, Guedes Soares C. Wave energy assessments in the Azores Islands. Renew
579 Energy 2012;45:183-96.

580 [16] van Nieuwkopp JCC, Smith HCM, Smith GH. Wave resource assessment along the
581 Cornish coast (UK) from a 23-year hindcast dataset validated against buoy measurements.
582 Renew Energy 2013;58:1-14.

583 [17] Rute Bento A, Martinho P, Guedes Soares C. Numerical modelling of the wave energy in
584 Galway Bay. Renew Energy 2015;78:457-66.

585 [18] Sierra JP, Martín C, Mösso C, Mestres M, Jebbad R. Wave energy potential along the
586 Atlantic coast of Morocco. Renew Energy 2016;96:20-32.

587 [19] Rusu E, Guedes Soares C. Numerical modelling to estimate the spatial distribution of
588 the wave energy in the Portuguese nearshore. Renew Energy 2009;34:1501-16.

589 [20] Silva D, Rute Bento A, Martinho P, Guedes Soares C. High resolution local wave energy
590 modelling in the Iberian Peninsula. Energy 2015;91:1099-112.

591 [21] Henriques JCC, Candido JJ, Pontes MT, Falcao AFO. Wave energy resource
592 assessment for a breakwater-integrated oscillating water column plant at Porto, Portugal.
593 Energy 2013;63:52-60.

594 [22] Iglesias G, Carballo R. Choosing the site for the first wave farm in a region: A case study
595 in the Galician Southwest (Spain). Energy 2011;36:5525-31.

596 [23] Iglesias G, Carballo R. Offshore and inshore wave energy assessment: Asturias (N
597 Spain). Energy 2010;35:1964-72.

598 [24] Iglesias G, Carballo R. Wave energy and nearshore hot spots: The case of the SE Bay
599 of Biscay. Renew Energy 2010;35:2490-500.

600 [25] Gonçalves M, Martinho P, Guedes Soares C. Wave energy conditions in the western
601 French coast. Renew Energy 2014;62:155-63.

602 [26] Gillou N. Evaluation of wave energy potential in the Sea of Iroise with two spectral
603 models. Ocean Eng 2015;106:141-51.

[27] Neill SP, Hashemi MR. Wave power variability over the northwest European shelf seas. Appl Energ 2013;106:31-46.

[28] Besio G, Mentaschi L, Mazzino A. Wave energy resource assessment in the Mediterranean Sea on the basis of a 35-year hindcast. Energy 2916;94:50-63.

[29] Mackay E, Bahaj A, Challenor P. Uncertainty in wave energy resource assessment. Part 2: Variability and predictability. Renew Energy 2010;35:1809-19.

[30] Reguero BG, Losada IJ, Méndez, FJ. A global wave power resource and its seasonal, interanual and long-term variability. Appl Energ 2015;148:366-80.

[31] Portilla J, Sosa J, Cavalieri L. Wave energy resources: wave climate and exploitation. Renew Energy 2013;57:594-605.

[32] Ching-Piao T, Ching-Her H, Chien H, Hao-Yuan C. Study oo the wave climate variation to the renewable wave energy assessment. Renew Energy 2012;38:50-61.

[33] Neill SP, Lewis MJ, Hashemi MR, Slater E, Lawrence J, Spall SA. Inter-annuak and inter-seasonal variability of the Orkney wave power resource. Appl Energ 2014;132:339-348.

[34] Falcao A. Wave energy utilization: a review of the technologies. Renew Sustain Energy Rew 2010;14:899-918.

[35] Mackay E, Bahaj A, Challenor P. Uncertainty in wave energy resource assessment. Part 1: Historic data. Renew Energy 2010;35:1792-808.

[36] Woolf D, Challenor PG. Variability and predictability of the North Atlantic wave climate. J Geophys Res 2002;107(C10):3145.

[37] Lionello P, Sanna A. Mediterranean wave climate variability and its link with NAO and Indian monsoon. Clim Dynam 2005;25:611-23.

[38] Hemer M, Church J, Hunter J. Variability and trends in the directional wave climate of the Southern Hemisphere. Int J Climatol 2010;30:475-91.

[39] Semedo A, Suselj K, Rutgersson A, Sterl A. A global view on the wind sea and swell climate and variability from ERA-40. J Clim 2011;24:1461-79.

[40] Guedes Soares C. Hindcast of dynamic processes of the ocean and coastal areas of Europe. Coast Eng 2008;55:825-6.

[41] Pilar P, Guedes Soares C, Carretero JC. 44-year wave hindcast for the north east Atlantic European coast. Coast Eng 2008;55:861-71.

[42] The WAMDI Group, The WAM model - a third generation ocean wave prediction model. J Phys Oceanogr 1988;18:1775-810.

[43] Jacob D. A note to the simulation of the annual and inter-annual variability of the water budget over the Baltic Sea drainage basin. Meteorol Atmos Phys 2001;77:61-73.

[44] Musić S, Nicković S. 44-year wave hindcast for the Eastern Mediterranean. Coast Eng 2008;55:872-80.

652 [45] Sotillo MG, Ratsimandresy AW, Carretero JC, Bentamy A, Valero F, González-Rouco F.
653 A high resolution 44-year atmospheric hindcast for the Mediterranean Basin: contribution to
654 the regional improvement to global reanalysis. Clim Dyn 2005;25:219-36.

655 [46] Ratsimandresy AW, Sotillo MG, Carretero JC, Álvarez-Fanjul E, Haiji HA. 44- year high
656 resolution ocean and atmospheric hindcast for the Mediterranean Basin developed within the
657 HIPOCAS project. Coast Eng 2008;55:827-42.

658 [47] Lynch P, Huang X-Y. Initialization of the HIRLAM model using a digital filter. Mon
659 Weather Rev 1992;120:1019-34.

660 [48] Sierra JP, Mösso C, González-Marco D. Wave energy resource assessment in Menorca
661 (Spain). Renew Energy 2014;71:51-60.

662 [49] Cornett, A global wave energy resource assessment. In International Offshore and Polar
663 Engineering Conference, Vancouver, Canada; 2008, p. 318-26.

664 [50] Henderson R, Design R. Simulation and testing of a novel hydraulic power take-off
665 system for the Pelamis wave energy converter. Renew Energy 2006;31:271-83.
666
667 [51] Kofoed JP, Frigaard P, Friis-Madsen E, Sørensen HC. Prototype testing of the wave
668 energy converter wave dragon. Renew Energy 2006;31:181-9.
669

670 **Figures**

671

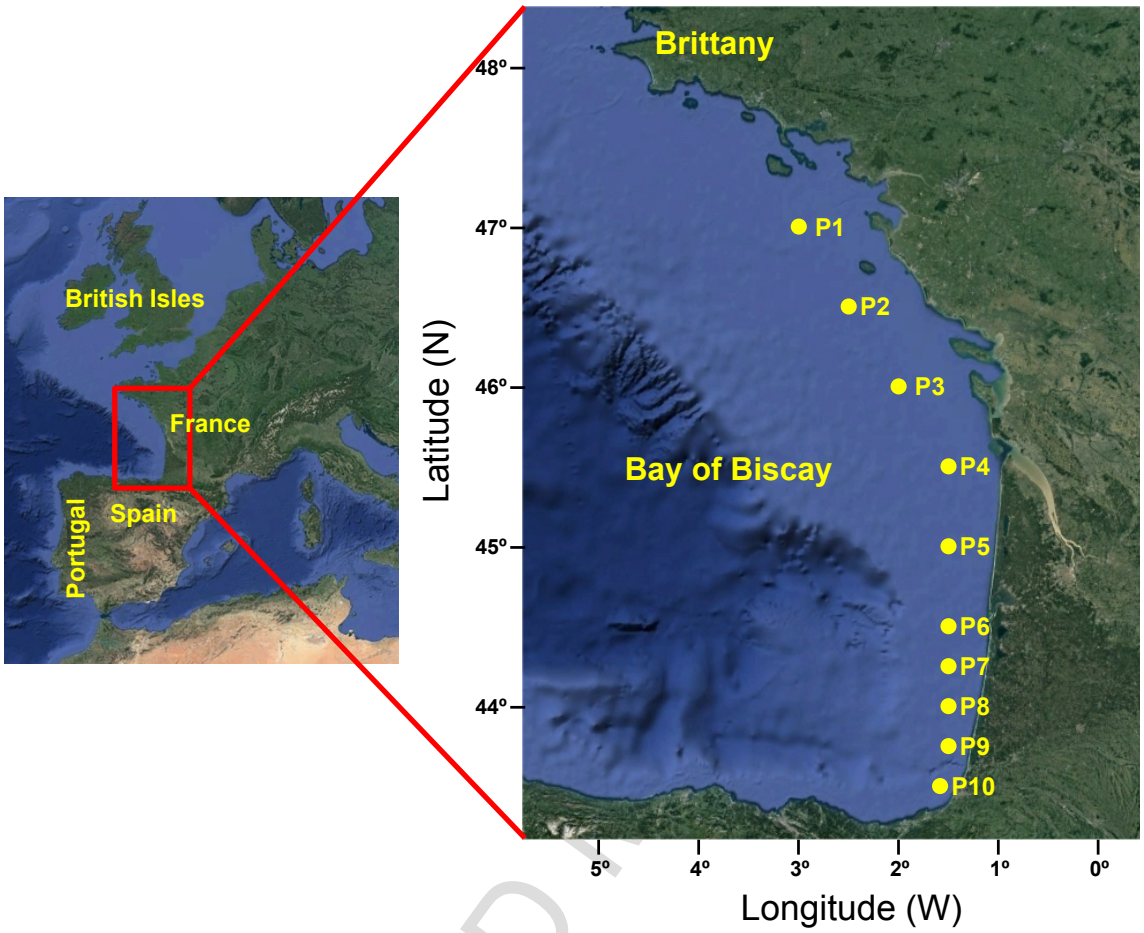

672

673 Figure 1. Map of the Bay of Biscay with the location of the 10 studied sites (adapted from Google Earth).
674

675
676

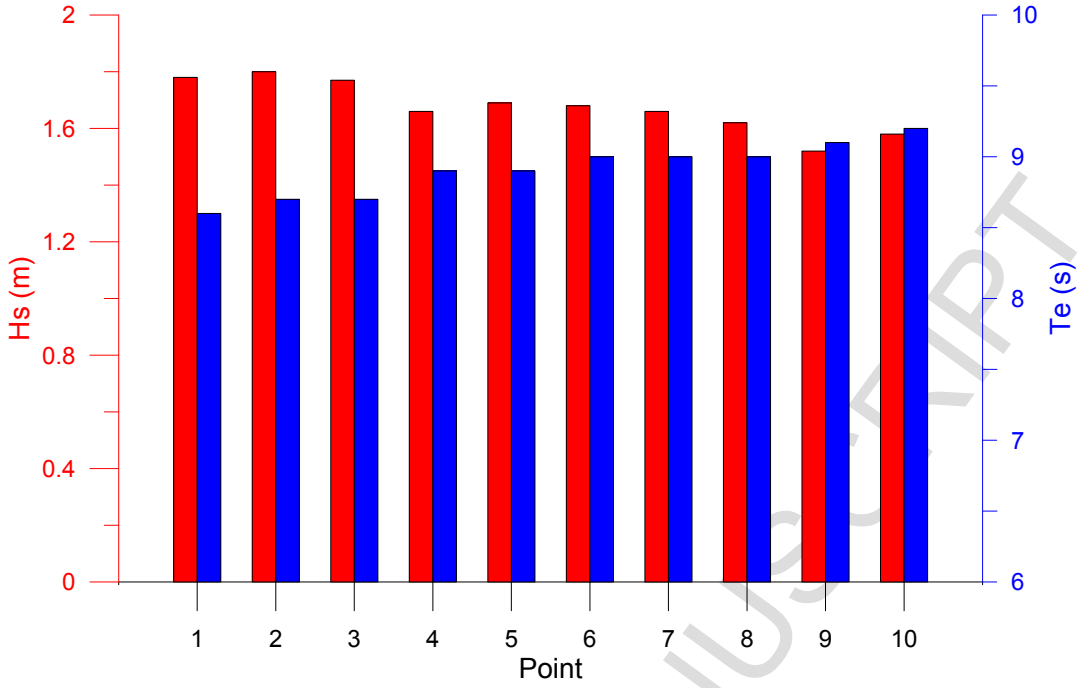

677

678 Figure 2. Values of the mean H_s and mean T_e for the 58-year period at the 10 studied sites.
679

680
681

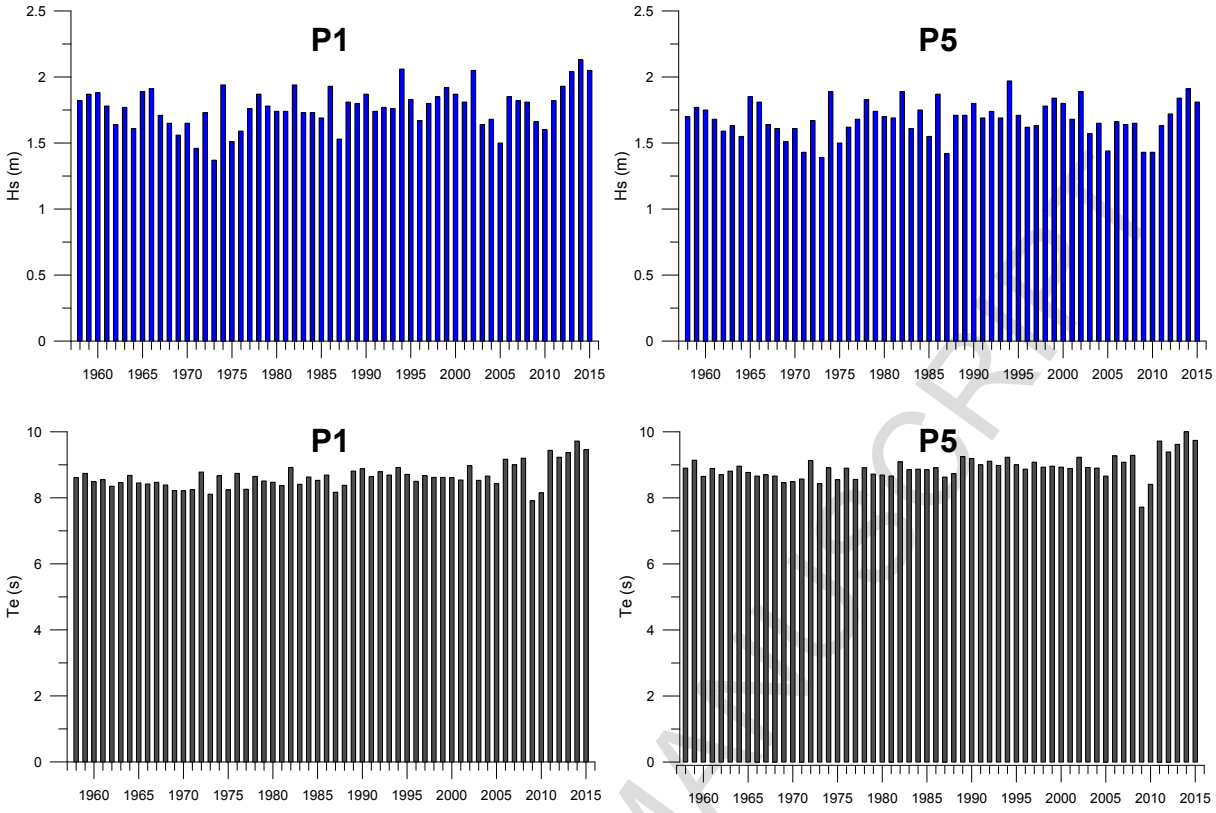

682

683 Figure 3. Average annual Hs (upper panels) and Te (lower panels) for every year at point P1 (left column) and P5
684 (right column).
685

686

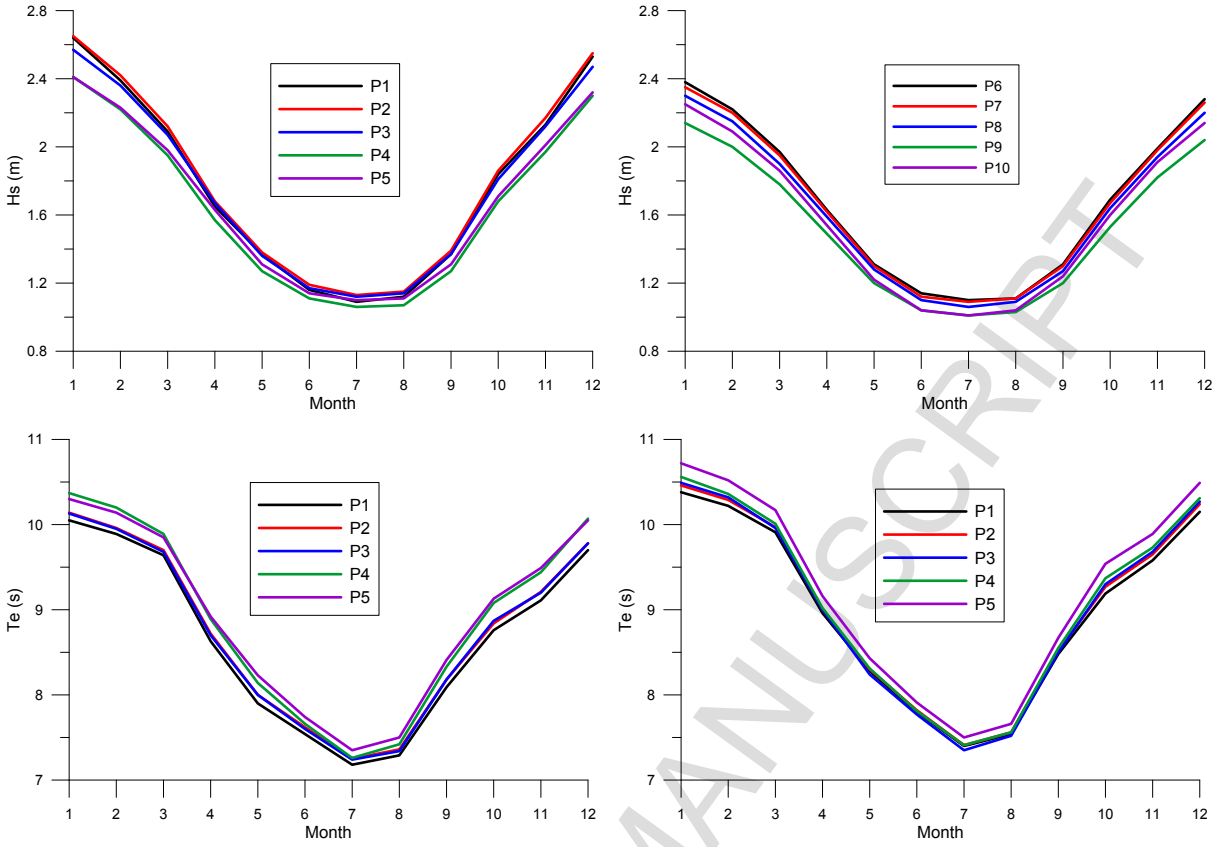

687

688 Figure 4. Monthly Hs (upper panels) and Te (lower panels) at the 10 studied locations, showing the average
689 values for the 58-year period.
690

691

692

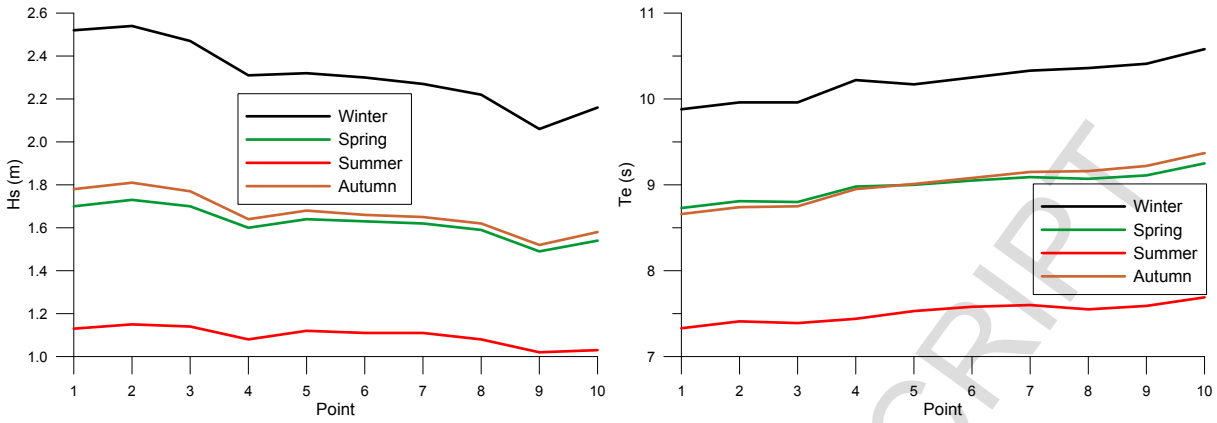

693

694 Figure 5. Seasonal Hs (left) and Te (right) at the 10 studied locations, showing the average values for the 58-year
695 period.

696

697

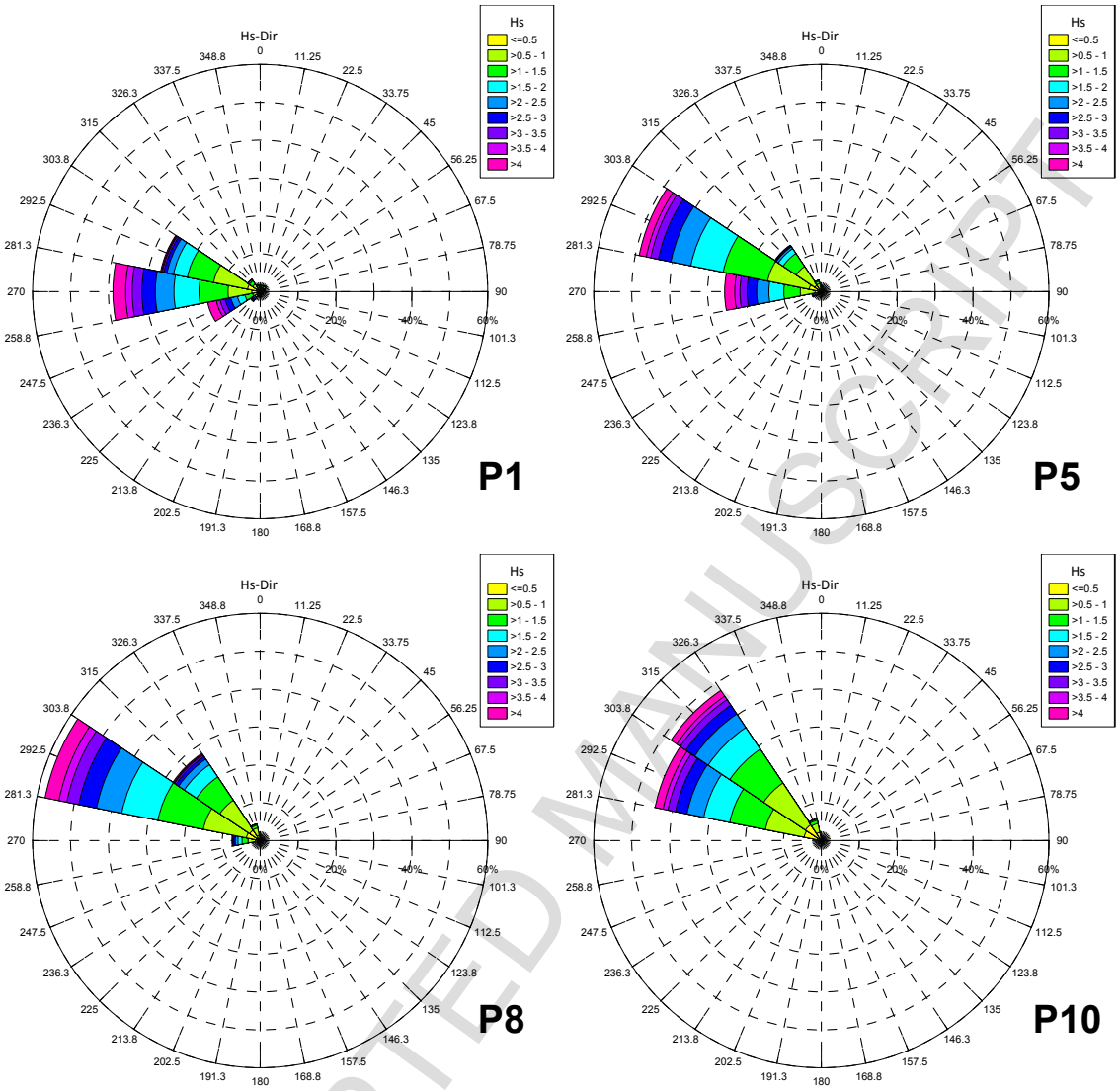

Figure 6. Wave roses corresponding to points P1, P5, P8 and P10 for the entire period (58 years).

703

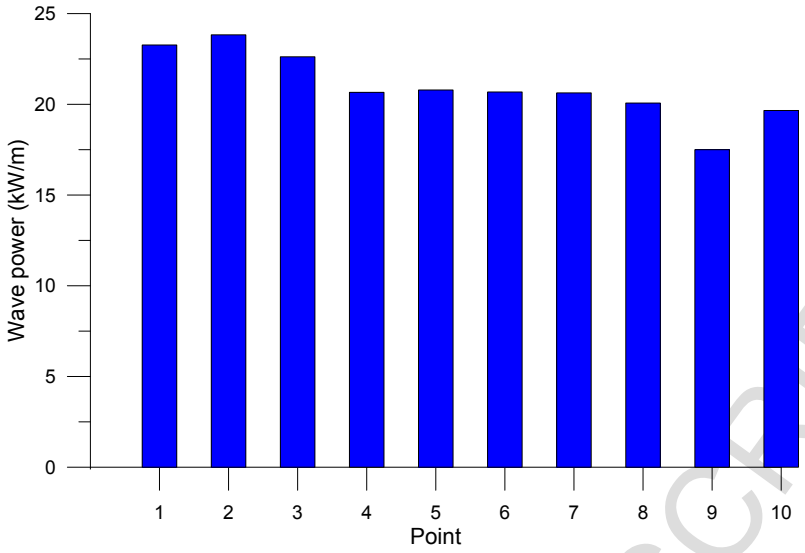

704

705 Figure 7. Average values (for the 58-year period) of the wave power at the 10 studied locations.
706

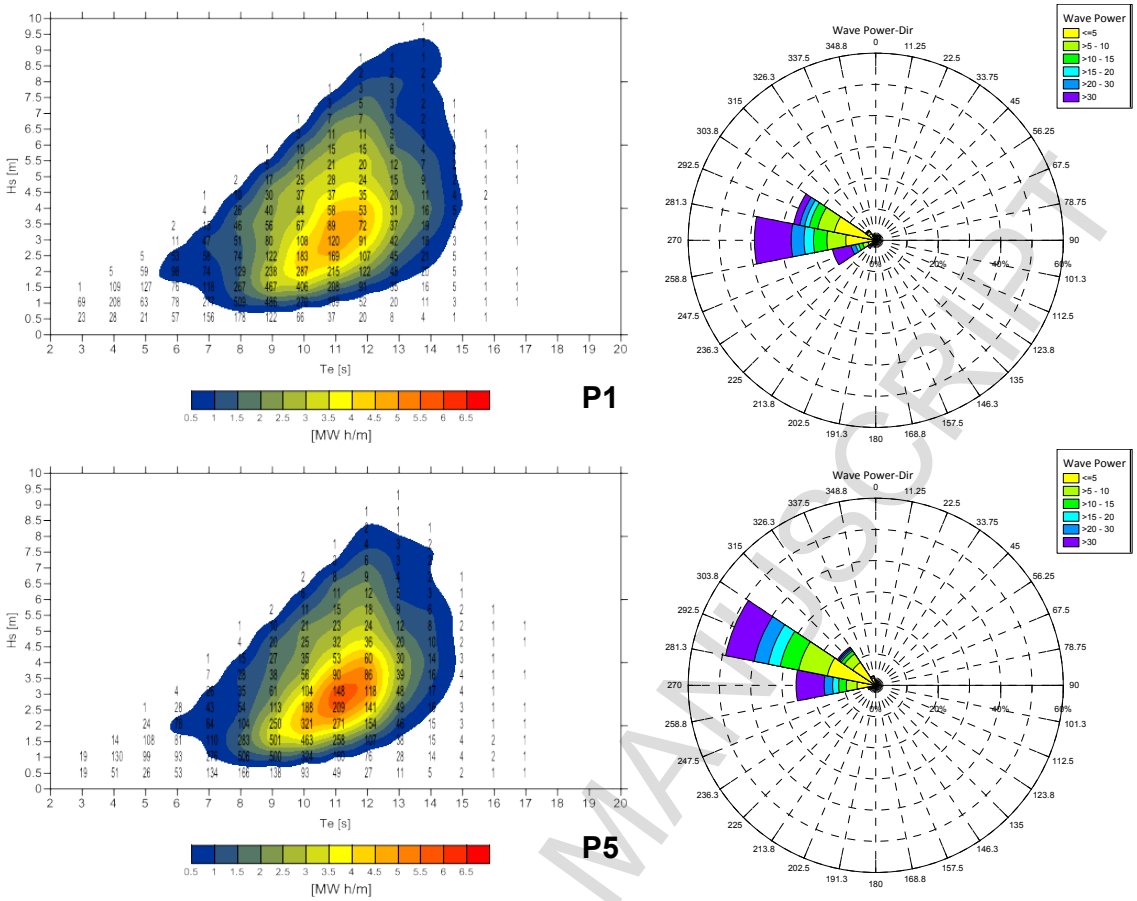

Figure 8. Energy roses and scatter diagrams indicating the different sea states' contribution to the total annual energy at points P1 and P5. Numbers indicate total energy (MW h/m).

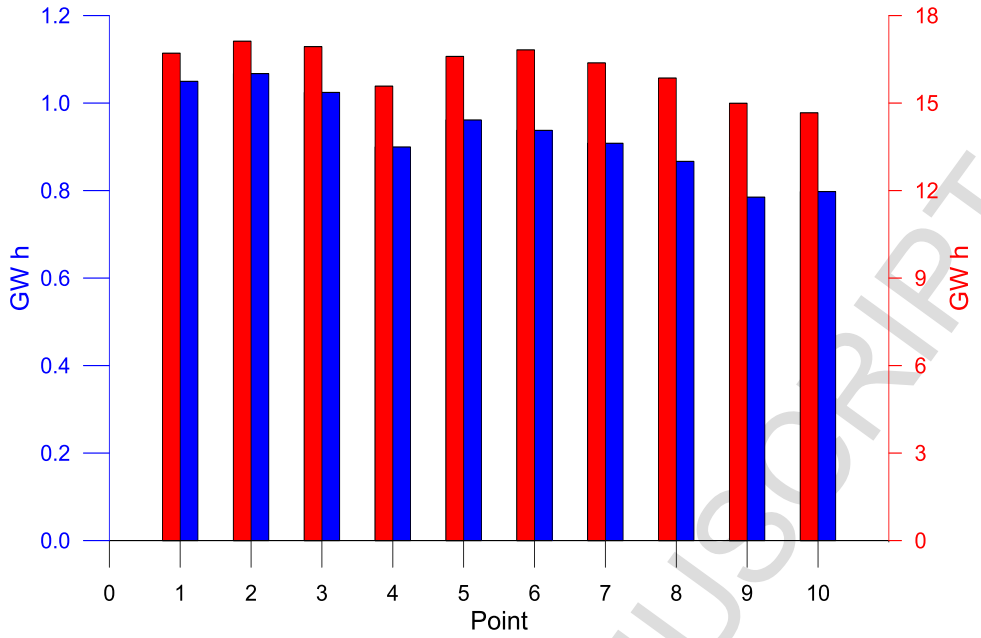

Figure 9. Annual average energy output (for the 58-year period) for both analyzed WECs: Wave Dragon (red) and Pelamis (blue) at the 10 studied points.

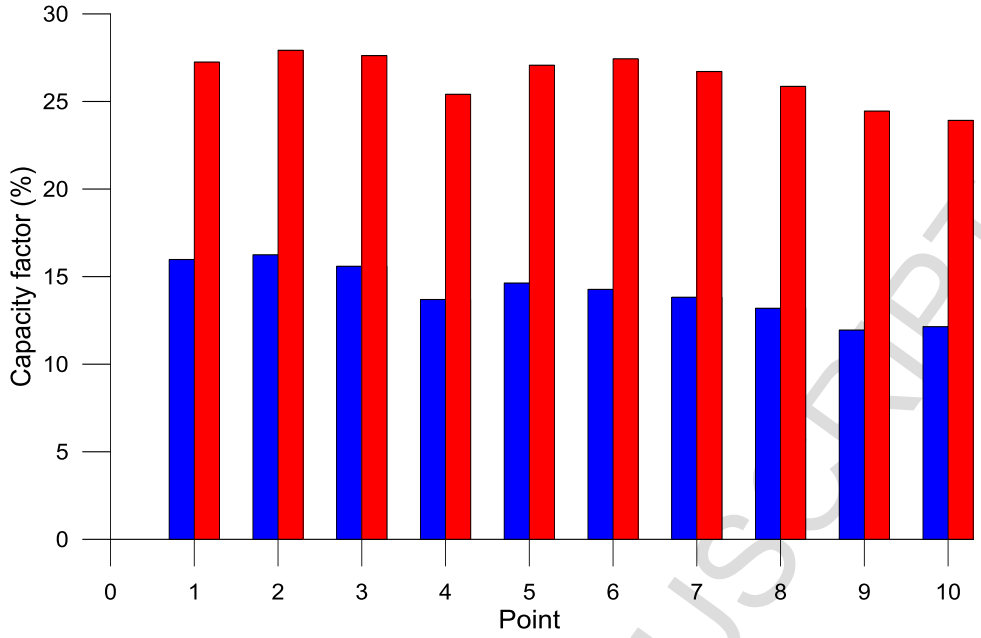

Figure 10. Average capacity factors (for the 58-year period) for both analyzed WECs: Wave Dragon (red) and Pelamis (blue) at the 10 studied sites.

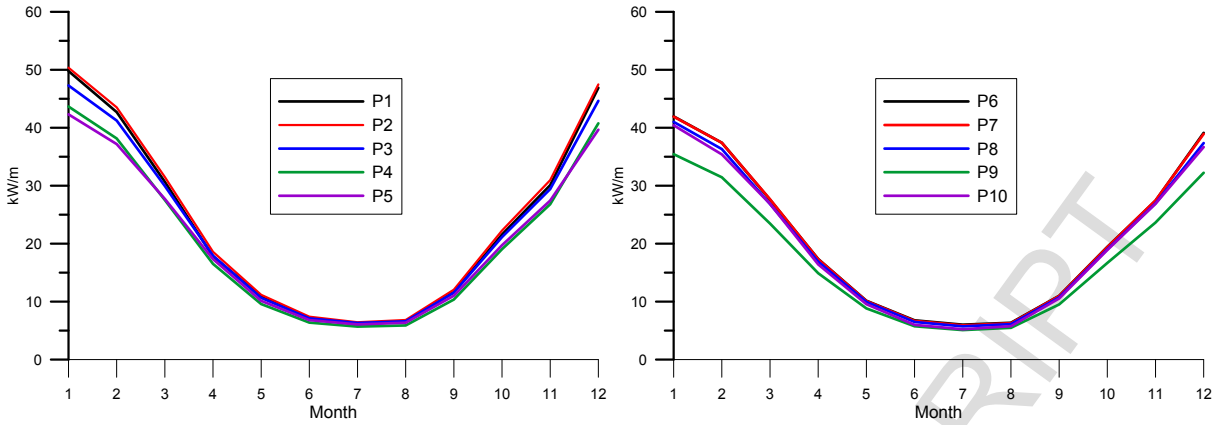

Figure 11. Monthly wave power (average values for the 58-year period) at the 10 studied locations.

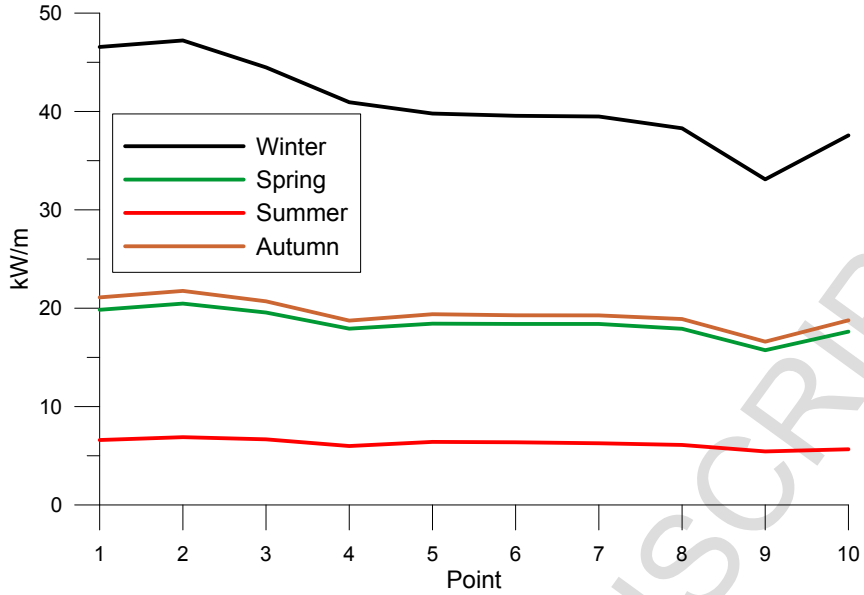

Figure 12. Seasonal wave power (average values for the 58-year period) at the 10 studied locations.

740

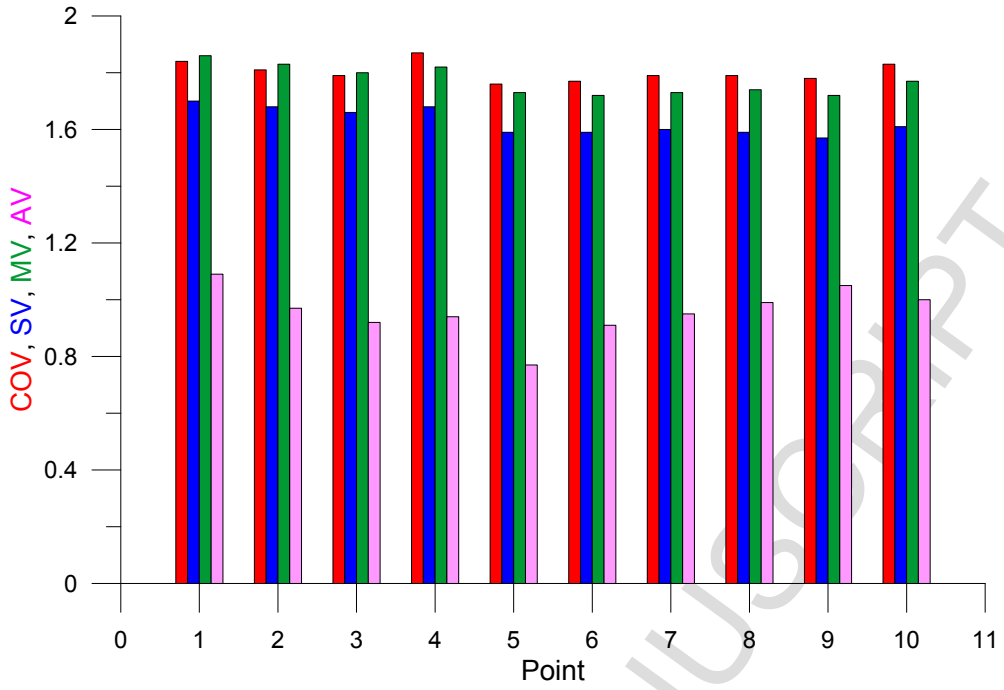

741

742 Figure 13. Variability coefficients at the 10 studied sites: COV (red), SV (blue), MV (green) and AV (pink).
743

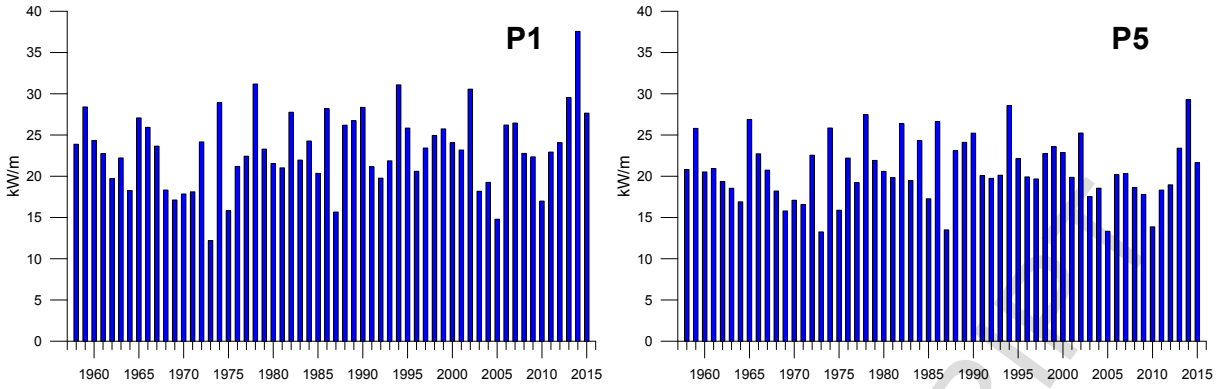

Figure 14. Average annual wave power for every year at point P1 (left) and P5 (right).

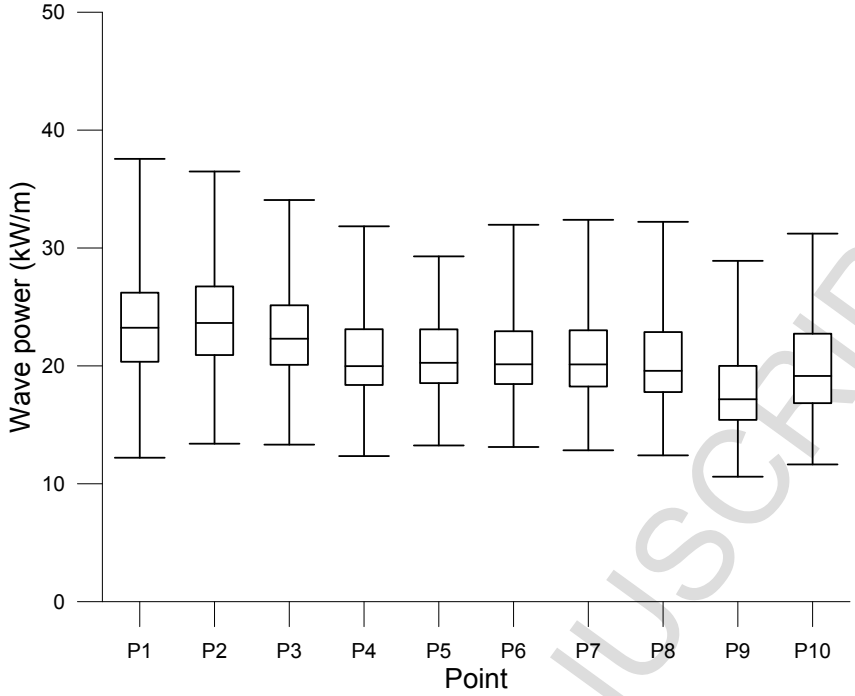

Figure 15. Box-whisker plots of the average annual wave power (for the 58-year period) at each point, showing its distribution broken into quartiles.

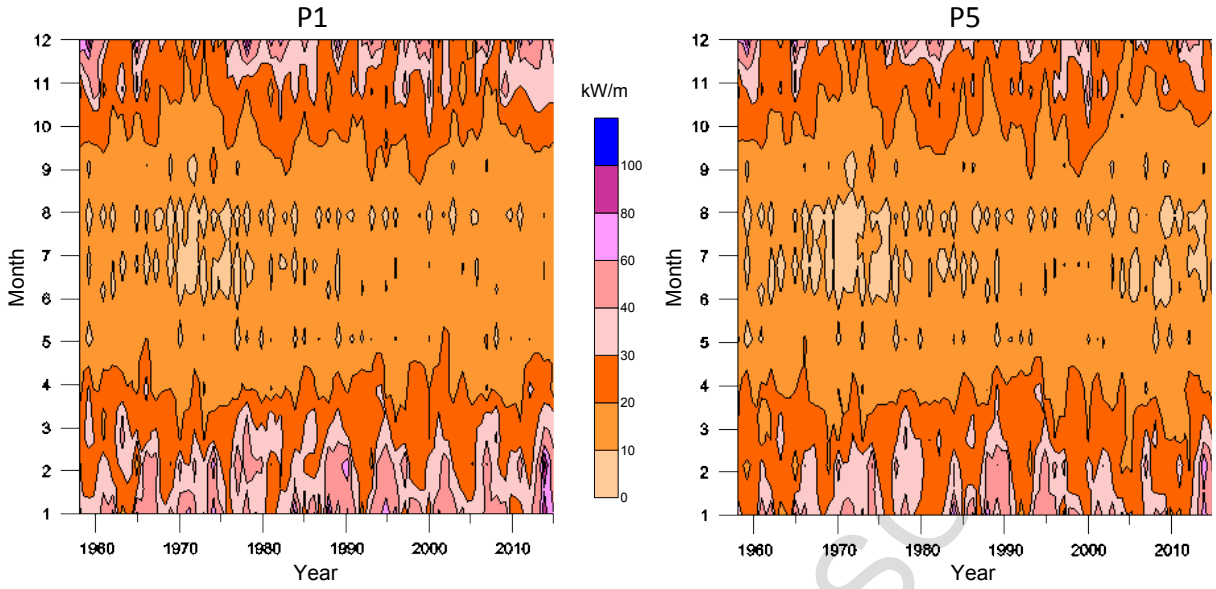

Figure 16. Overall variability of the mean wave power over the months and over the years at points P1 (left) and P5 (right).

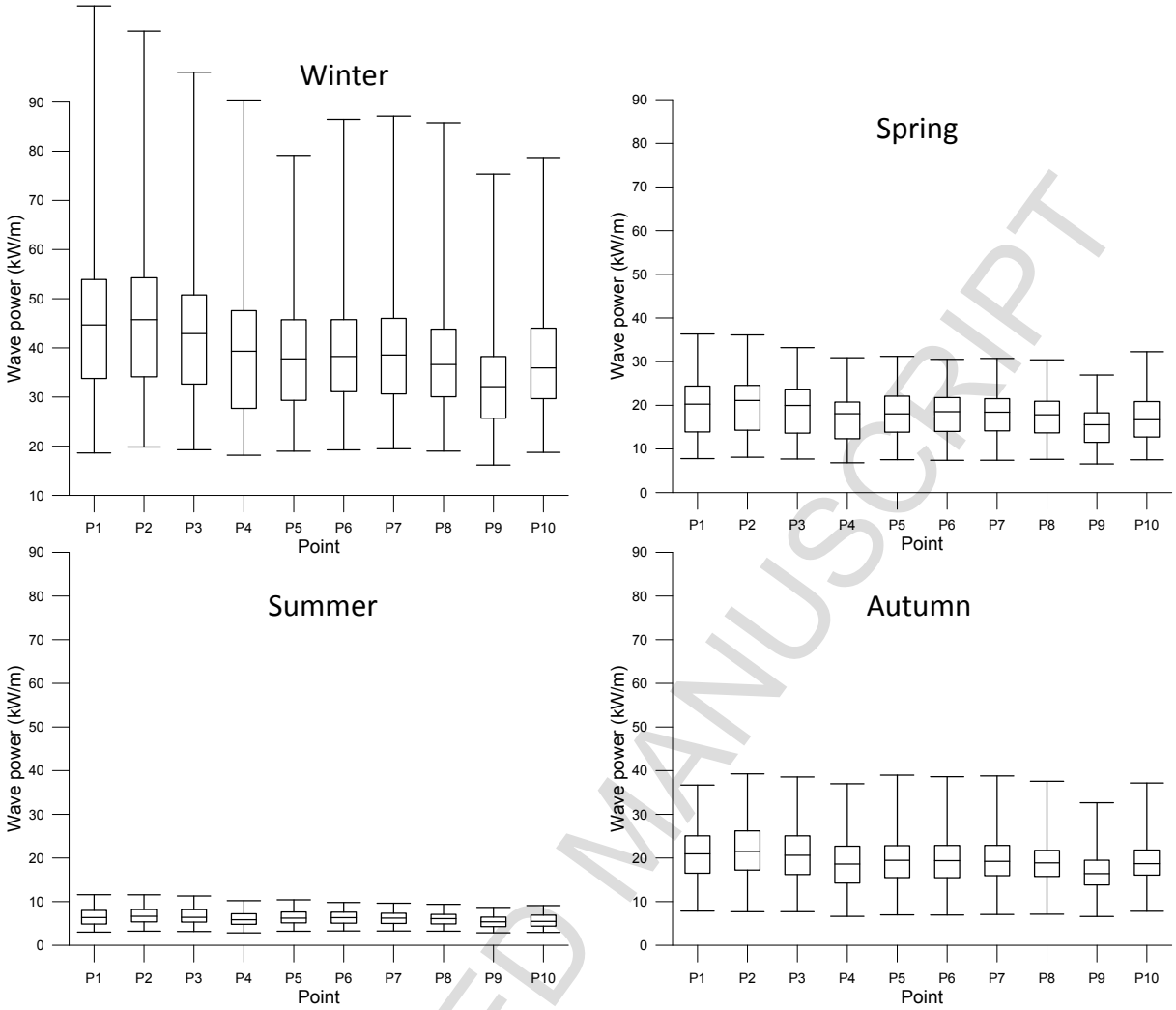

Figure 17. Box-whisker plots obtained at each point from the yearly values of the seasonal wave power.

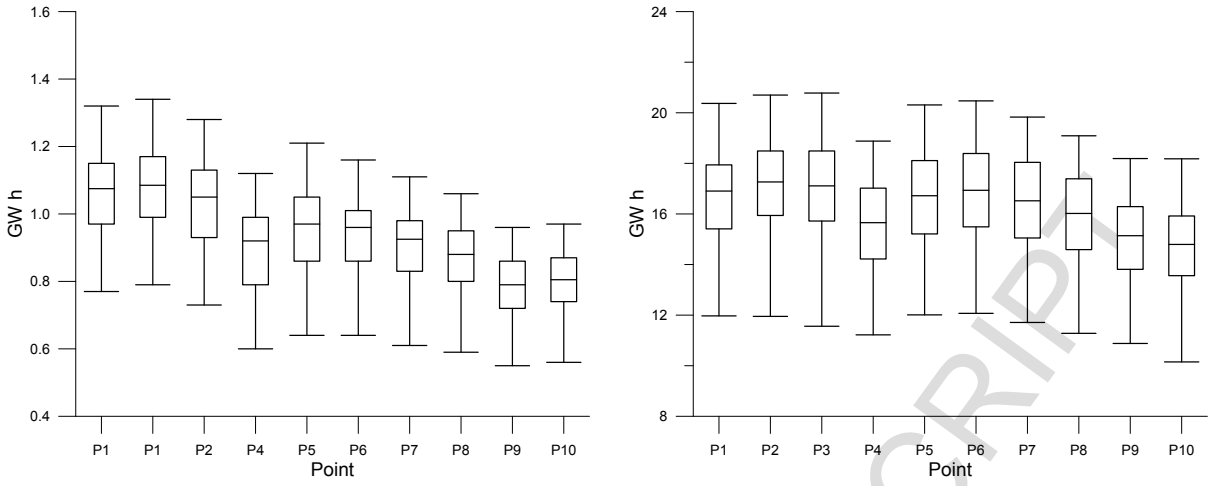

Figure 18. Box-whisker plots obtained at each point from the yearly values of the energy output for Pelamis (left) and Wave Dragon (right) WECs.

781
782 **Tables**
783
784

Point	Mean power (kW/m)	Annual Energy (MW h/m)	Annual energy output (GW h)		Capacity factor (%)	
			Pelamis	Wave Dragon	Pelamis	Wave Dragon
P1	23.27	203.85	1.05	16.71	15.98	27.25
P2	23.83	208.75	1.07	17.02	16.25	27.92
P3	22.62	198.15	1.02	16.94	15.59	27.62
P4	20.66	180.98	0.90	15.58	13.69	25.41
P5	20.79	182.12	0.96	16.60	14.63	27.07
P6	20.68	181.16	0.94	16.82	14.27	27.44
P7	20.63	180.72	0.91	16.38	13.82	26.71
P8	20.07	175.81	0.87	15.86	13.19	25.86
P9	17.50	153.30	0.79	14.99	11.95	24.45
P10	19.66	172.22	0.80	14.67	12.14	23.92

785

786 Table 1. Wave power, energy potential, annual average energy output and capacity factors for both analyzed
787 WECs at the 10 studied points (averages for the 58-year period).
788

789

790

Point	COV	SV	MV	AV
P1	1.84	1.70	1.86	1.09
P2	1.81	1.68	1.83	0.97
P3	1.79	1.66	1.80	0.92
P4	1.87	1.68	1.82	0.94
P5	1.76	1.59	1.73	0.77
P6	1.77	1.59	1.72	0.91
P7	1.79	1.60	1.73	0.95
P8	1.79	1.59	1.74	0.99
P9	1.78	1.57	1.72	1.05
P10	1.83	1.61	1.77	1.00

791

792 Table 2. Variability coefficients at the 10 studied locations.
793

794

Point	P_{year} (kW/m)	P_{Y1} (kW/m)	P_{Y58} (kW/m)	P_{Y1}/P_{Y58}
P1	23.27	37.56	12.21	3.08
P2	23.83	36.49	13.40	2.72
P3	22.62	34.07	13.32	2.56
P4	20.66	31.84	12.35	2.58
P5	20.79	29.29	13.25	2.21
P6	20.68	31.97	13.12	2.44
P7	20.63	32.39	12.84	2.52
P8	20.07	32.22	12.41	2.60
P9	17.50	28.91	10.60	2.73
P10	19.66	31.22	11.64	2.68

Table 3. Wave power annual variability at each point, with the mean annual energy during the 58-year period (P_{year}), the mean annual energy in the most energetic year (P_{Y1}) and the less energetic one (P_{Y58}) and the ratio between both.

Point	P_{M1} (kW/m)	P_{M696} (kW/m)	P_{M1}/P_{M696}	P_{MY1}/P_{MY12}
P1	150.74	0.95	158.67	21.35 (7.05 , 74.05)
P2	144.17	1.19	121.15	19.91 (6.88 , 65.42)
P3	133.38	1.31	101.82	18.66 (6.43 , 59.34)
P4	124.09	1.30	95.45	19.36 (6.51 , 60.40)
P5	112.40	1.67	67.31	16.82 (6.30 , 44.66)
P6	116.00	1.81	64.09	16.41 (6.13 , 41.62)
P7	115.73	1.89	61.23	16.55 (6.21 , 40.14)
P8	112.70	2.04	55.25	16.29 (6.20 , 37.55)
P9	98.29	1.62	60.67	16.16 (6.07 , 40.26)
P10	111.36	1.71	65.12	17.71 (6.96 , 41.81)

Table 4. Wave power monthly variability at each point, with the maximum monthly energy in the 58 years (P_{M1}), the minimum one (P_{M696}), the ratio between both (P_{M1}/P_{M696}), and ratios between the most and the less energetic months in the same year (P_{M1}/P_{M12}), where the first value indicates the average of the 58 years and the values between brackets the range of variation.

Point	P_{WI} (kW/m)	P_{SP} (kW/m)	P_{SU} (kW/m)	P_{AU} (kW/m)	P_{S1}/P_{S4}
P1	18.62 , 109.55	7.78 , 36.33	3.02 , 11.59	7.84 , 36.70	7.66 (2.44 , 17.92)
P2	19.84 , 104.45	8.10 , 36.12	3.24 , 11.57	7.69 , 39.26	7.40 (2.42 , 17.07)
P3	19.27 , 96.07	7.69 , 33.21	3.17 , 11.30	7.70 , 38.55	7.17 (2.41 , 16.53)
P4	18.15 , 90.42	6.83 , 30.89	2.85 , 10.22	6.63 , 37.00	7.33 (2.40 , 17.79)
P5	18.98 , 79.16	7.54 , 31.21	3.23 , 10.42	6.97 , 38.97	6.62 (2.29 , 14.87)
P6	19.25 , 86.49	7.40 , 30.53	3.29 , 9.81	6.94 , 38.61	6.59 (2.22 , 15.52)
P7	19.48 , 87.14	7.41 , 30.74	3.28 , 9.64	7.06 , 38.79	6.68 (2.25 , 15.90)
P8	19.00 , 85.80	7.62 , 30.42	3.24 , 9.39	7.12 , 37.57	6.66 (2.25 , 16.17)
P9	16.16 , 75.35	6.56 , 26.93	2.87 , 8.68	6.60 , 32.65	6.46 (2.18 , 15.34)
P10	18.74 , 78.73	7.52 , 32.28	2.96 , 9.10	7.80 , 37.17	7.08 (2.46 , 15.88)

Table 5. Wave power seasonal variability at each point, with the minimum and maximum winter (P_{WI}), spring (P_{SP}), summer (P_{SU}) and autumn (P_{AU}) values in the 58-year period, and ratios between the most and the less energetic seasons in the same year (P_{S1}/ P_{S4}), where the first value indicates the average of the 58 years and the values between brackets the range of variation.

Point	Pelamis			Wave Dragon		
	E_{max} (GW h)	E_{min} (GW h)	E_{max}/E_{min}	E_{max} (GW h)	E_{min} (GW h)	E_{max}/E_{min}
P1	1.32	0.77	1.71	20.37	11.97	1.70
P2	1.34	0.79	1.70	20.70	11.95	1.73
P3	1.28	0.73	1.75	20.78	11.56	1.80
P4	1.12	0.60	1.87	18.88	11.22	1.68
P5	1.21	0.64	1.89	20.31	12.01	1.69
P6	1.16	0.64	1.81	20.47	12.07	1.70
P7	1.11	0.61	1.82	19.83	11.71	1.69
P8	1.06	0.59	1.80	19.09	11.28	1.69
P9	0.96	0.55	1.75	18.19	10.88	1.67
P10	0.97	0.56	1.83	18.18	10.15	1.79

Table 6. Energy output variability at each point in the 58-year period for the two studied WECs (Pelamis and Wave Dragon), including the maximum (E_{max}) and minimum (E_{min}) annual values and the ratio between them (E_{max}/E_{min}).